Theoretical and Applied Fracture Mechanics 119 (2022) 103274

Contents lists available at ScienceDirect

Theoretical and Applied Fracture Mechanics

journal homepage: www.elsevier.com/locate/tafmec

Comparative analytical study of the coupled criterion and the principle of minimum total energy with stress condition applied to linear elastic interfaces

M. Muñoz-Reja, V. Mantič, L. Távara *

Grupo de Elasticidad y Resistencia de Materiales, Escuela Técnica Superior de Ingeniería, Universidad de Sevilla, Camino de los Descubrimientos s/n, 41092 Sevilla, Spain

ARTICLE INFO

Keywords:
Linear Elastic Brittle Interface Model (LEBIM)
Coupled criterion
Finite Fracture Mechanics (FFM)
Double cantilever beam test
Total energy minimization

ABSTRACT

In the present work the Coupled Criterion of Finite Fracture Mechanics (CCFFM) is used to predict crack onset or growth by finite increments in a linear elastic interface. The predictions of the interface failure by two alternative approaches of the CCFFM applied to the Linear Elastic Brittle Interface Model (LEBIM): the widely used method based on looking for an intersection of stress and energy criteria curves and the novel Principle of Minimum Total Energy subjected to a Stress Condition (PMTE-SC), are studied and compared. For this purpose, two analytical studies, based on the stress and energy criteria curves and the PMTE-SC, are carefully explained, providing appropriate graphical representations, by considering the widely used Double Cantilever Beam (DCB) test as benchmark problem. For the sake of simplicity, the Euler–Bernoulli beam model including an elastic interface (the Winkler interface) to model the adhesive layer joint is used in this study. To the authors' best knowledge, this is the first study showing, for both load and displacement control, that the PMTE-SC is equivalent to the classical formulation of the CCFFM, providing exactly the same analytical predictions for the crack onset and propagation. The fact that onset of a finite crack-advance typically predicted by CCFFM is associated to tunnelling the total energy barrier is also illustrated on the DCB test. The main advantages of the PMTE-SC are its versatility and possibility of applying it to complex configurations including multiple cracks and fracture mixed-mode behaviour.

1. Introduction

Finite Fracture Mechanics (FFM) theory assumes that the crack onset is produced (at the considered time scale apparently) instantly with a finite length. It may be caused by an abrupt coalescence of defects of the material for a critical value of the tension. Therefore, FFM does not maintain the Griffith hypothesis for the Linear Elastic Fracture Mechanics (LEFM) theory, which assumes that the crack growth is infinitesimal. This is why FFM is able to predict the onset of fracture in the form of a new finite crack segment even under a uniform stress field [1].

In the framework of the FFM, the Coupled Criterion of the FFM (CCFFM) was proposed [2]. This criterion combines two criteria traditionally used separately in brittle and quasi-brittle materials: the stress criterion and the energy criterion. The first one was commonly used to predict failure when stress singularities are not present, while the energy criterion was employed in the presence of cracks. There are many experimental evidences supporting the hypothesis by Leguillon, see e.g. [2–10].

On the other hand, interface conditions ahead of an interface crack front play a critical role when defining a crack growth model. The Linear Elastic-(perfectly) Brittle Interface Model (LEBIM) was proposed and studied in [11–14], among many others, to model cracks propagating on a weak surface/interface, which may represent, e.g., an adhesive layer. It is characterized by a continuous spring-distribution (often referred to as the Winkler interface) with a linear elastic-(perfectly) brittle law, which relates the displacement jump across this interface (material separation, in Mode I) and tractions acting there.

An improved constitutive law including a failure criterion of the LEBIM was introduced and analysed in [15–17]. This model covers also interface fracture due to shear under compression, by extending the range of variation of the interface fracture energy with the fracture mode mixity, and considering the possibility of frictionless elastic contact at broken portions of the interface.

Traditionally, LEBIM has been applied to characterize interfaces with a relatively low stiffness. This is because the fracture energy and

* Corresponding author.
E-mail addresses: mmunozreja@us.es (M. Muñoz-Reja), mantic@us.es (V. Mantič), ltavara@us.es (L. Távara).

https://doi.org/10.1016/j.tafmec.2022.103274
Received 12 October 2021; Received in revised form 10 January 2022; Accepted 26 January 2022
Available online 19 February 2022

critical tractions of an interface modelled by LEBIM are coupled by an equation involving the interface stiffness. However, such an interface model may be far from reality, especially for thin adhesive layers characterized by a large stiffness. Another disadvantage of the LEBIM is that it considers only infinitesimal propagation of damage, similarly to the LEFM. However, in some fracture processes, the failure occurs instantaneously, leading to a crack growth with a finite length. Due to these two facts, the CCFFM approach has been incorporated into LEBIM [18–22]. Using this new approach, it was possible to decouple the fracture energy, critical traction and stiffness of an interface.

The novelty of this work is the comparative study between two alternative approaches of the CCFFM. The first approach is the well-known method based on the stress and energy criteria curves which is used by most authors. The second approach is the novel Principle of Minimum Total Energy subjected to a Stress Condition (PMTE-SC) introduced in [23]. Moreover, several aspects and applications of PMTE-SC to the crack onset and propagation are analysed, assuming a quasistatic problem evolution (i.e. inertial forces are neglected). The Double Cantilever Beam (DCB) test is used as reference problem. Additionally, some analyses regarding the effect of the way the test is controlled (load or displacement control) are done using an analytical solution based on the beam theory models including an elastic interface. Noteworthy, the main advantage of the proposed methodology based on the PMTE-SC is its versatility and applicability to complex configurations with multiple cracks and mixed-mode fracture. This methodology can be implemented in a straightforward manner in a numerical tool based on FEM, eliminating the need to derive an analytical solution.

2. Theoretical framework of the CCFFM + LEBIM

Several authors [18,21,22,24,25] have previously applied the CCFFM to elastic interface models and described in detail the theoretical framework of this method. Thus, for the sake of brevity, the CCFFM + LEBIM formulation to be used in this paper is just briefly described in this section. As mentioned above, the present CCFFM is based on the interface strength and fracture energy criteria, each of them representing a necessary but not sufficient condition for a crack onset and/or growth.

The stress criterion is evaluated before the crack onset on the entire weak surface where the crack is expected to initiate or grow. However, in this method, as the coupled criterion is applied to elastic interfaces, the stress criterion is imposed for all undamaged points x at every interface component of the problem. The aim is to localize one or several finite segments of the interface which can be damaged, e.g. from $x = 0$ to $x = \Delta a$, satisfying the stress criterion. This condition can be written as:

$$\frac{t(x)}{t_c(\psi(x))} \geq 1, \quad \text{for all } x, \quad 0 \leq x \leq \Delta a, \tag{1}$$

$$\text{with} \quad t(x) = \sqrt{\sigma^2(x) + \tau^2(x)} \quad \text{and} \quad t_c(\psi(x)) = \sqrt{\sigma_c^2(\psi(x)) + \tau_c^2(\psi(x))},$$

where $\sigma(x)$ and $\tau(x)$ are the normal and shear stress components at an undamaged interface point x, and $t(x)$ is the traction vector modulus. $\sigma_c(\psi(x))$ and $\tau_c(\psi(x))$ are the maximum allowed stress components at x giving the critical traction vector modulus $t_c(\psi(x))$, which can be defined by several suitable stress criteria (similarly to LEBIM) and depends on the fracture mode-mixity angle $\psi(x)$ at x [17], see also [22] for a deeper analysis of the formulation. The critical normal and shear stress components can be defined by dimensionless functions as proposed in [17]:

$$\sigma_c(\psi) = \sigma_{c,ch}\hat{\sigma}_c(\psi) \quad \text{and} \quad \tau_c(\psi) = \sigma_{c,ch}\hat{\tau}_c(\psi), \tag{2}$$

where $\sigma_{c,ch}$ is a characteristic interface strength parameter, e.g., for cracks growing in pure mode I (as in the DCB test) $\sigma_{c,ch}$ becomes the tensile strength of the interface σ_c. Then, the dimensionless critical traction vector modulus is defined by $t_c(\psi(x)) = \sigma_{c,ch}\hat{t}_c(\psi(x))$.

Following the dimensionless and general formulation introduced in [23], the (pointwise) stress criterion can be written in general form, as

$$\frac{\sigma_{nom}}{\sigma_{c,ch}} \geq s(x) = \frac{\hat{t}_c(\psi(x))}{\hat{t}(x)}, \quad \text{for all } x \in [0, \Delta a], \tag{3}$$

where σ_{nom} is the applied nominal stress which depends on the problem and represents the external loads, and $t(x) = \sigma_{nom}\hat{t}(x)$.

In addition to the stress criterion, to initiate or propagate an interface crack by a finite increment of its length $\Delta a > 0$, the following energy balance condition must be fulfilled

$$-\Delta\Pi(\Delta a) \geq \Delta R(\Delta a), \tag{4}$$

where the left and right hand sides are defined as the decrement of the potential energy and the increment of the dissipated energy, respectively, at this (typically instantaneous) finite crack-advance Δa. The energy released in the fracture process can be computed by several methods, its suitability may depend on the CCFFM approach used, e.g., calculating either the integral of the ERR considering a virtual crack growing on the interface part defined by Δa [17,19,21], or the decrement of potential energy by subtracting the potential energies before and after the interface failure [23].

Following [23,26,27], the energy condition for linear elastic materials can be written in terms of dimensionless functions as follows

$$-\frac{\sigma_{nom}^2 l_{ch}^2}{2k_{ch}}\Delta\hat{\Pi}(\Delta\alpha) \geq G_{c,ch} l_{ch}^2 \Delta\hat{R}(\Delta\alpha), \tag{5}$$

where l_{ch} is a characteristic length of the problem, $\Delta\alpha = \frac{\Delta a}{l_{ch}}$, σ_{nom} is the applied nominal stress (as considered in the stress criterion), and $\hat{\Pi}$ and $\hat{R}$ are dimensionless functions. Additionally, $G_{c,ch}$ is the characteristic fracture-energy of the interface, and k_{ch} is the characteristic stiffness of the interface, becoming the fracture energy of the interface G_{Ic} and the normal stiffness of the interface k_n, respectively, for pure mode I.

Following the formulation of the CCFFM introduced in [26], the dimensionless function $g(\Delta\alpha)$ can be defined as

$$g(\Delta\alpha) = \frac{\Delta\hat{R}(\Delta\alpha)}{-\Delta\hat{\Pi}(\Delta\alpha)}. \tag{6}$$

Following [18,19,21,22], an adequate way to represent the relation between the critical stress, the fracture energy and the stiffness of the interface in pure mode I, is the one represented in Fig. 1, see [19], where it can be seen that the dimensionless parameter

$$\mu = \frac{2G_{Ic}\,k_n}{\sigma_c^2} = \left(\frac{\sigma_{max}}{\sigma_c}\right)^2 = \left(\frac{\delta_{max}}{\delta_c}\right)^2 \tag{7}$$

characterizes the interface brittleness or toughness in mode I in CCFFM + LEBIM. Note that σ_{max} and σ_c are the maximum and critical tensions associated with the energy and stress based criteria, and similarly δ_{max} and δ_c are the maximum and critical normal relative displacements associated with the energy and stress based criteria, respectively.

If G_{Ic} and σ_c are considered constant, then the interface becomes stiffer when μ value increases, and the perfect interface (with vanishing relative displacements on undamaged parts) is recovered for $\mu \to \infty$.

Finally, the energy criterion can be rewritten as

$$\frac{\sigma_{nom}}{\sigma_c} \geq \sqrt{\mu\, g(\Delta\alpha)}. \tag{8}$$

If the stress criterion in (3) is expressed as a function of the dimensionless finite segment of the crack, $\Delta\alpha$, like in the energy criterion (8), the CCFFM applied to LEBIM can be written as

$$\frac{\sigma_{nom,c}}{\sigma_c} = \min_{\Delta\alpha} \max \left\{ s(\Delta\alpha), \sqrt{\mu\, g(\Delta\alpha)} \right\}, \tag{9}$$

where $\sigma_{nom,c}$ is the minimum load that satisfies both criteria and produces a crack with length $\Delta\alpha = \Delta\alpha_c$.

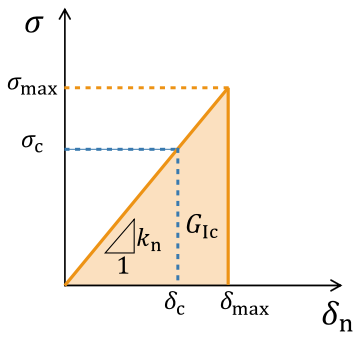

Fig. 1. CCFFM + LEBIM constitutive law in pure mode I.

It is interesting to recall that some authors related the behaviour of the bi-linear traction separation law, in the framework of the well-known Cohesive Zone Model (CZM), and the Coupled Criterion of Finite Fracture Mechanics (CCFFM) for elastic interfaces [14,18]. Although the physical effect in both approaches is similar (i.e. an increase in μ leads to a more ductile behaviour of the interface), their mathematical definition is different. In a bi-linear traction separation law the stiffness changes (being a function of the damage parameter) while in the CCFFM approach the stiffness remains unaltered until the breakage of a portion of interface happens when this stiffness suddenly jumps down to zero. Let us recall that, the mechanical characterization of the interface in the CCFFM approach is based on two hypotheses:

- CCFFM does not follow Griffith hypothesis, where an infinitesimal crack growth is assumed. Thus, the energy balance is defined incrementally, and a finite crack growth can be predicted.
- Both, the stress- and energy-based criteria must be fulfilled simultaneously. The stress-based criterion establishes a condition on the traction vector along the possible crack path (prior to the crack generation). The energy-based criterion is based on the incremental energetic balance between the state prior and after the instantaneous crack formation.

These assumptions allow modelling the interface failure in the linear-elastic framework and using the same value of the stiffness of the undamaged part of the interface until a certain moment, when this stiffness jumps down in the instantaneous crack growth process (i.e., without a presence of a softening zone).

Note that, for $\Delta\alpha \to 0$ the functions $s(\Delta\alpha)$ and $g(\Delta\alpha)$ represent the original LEBIM if the same failure criterion is used. This is due to the equivalence between the Energy Release Rate (ERR) and the tractions, and the equivalence between the fracture energy and critical tractions, at a particular unbroken interface-point, as showed in [17]. This equivalence implies that for $\Delta\alpha \to 0$ and $\mu = 1$ the CCFFM+LEBIM reverts to the original LEBIM, due to the characterization of the interface failure represented by $\mu = 1$, and by the infinitesimal propagation of the LEBIM $\Delta\alpha \to 0$. These two features of the original LEBIM highlight the two main reasons for the application of CCFFM to LEBIM:

- In CCFFM+LEBIM it is possible to uncouple the fracture toughness, critical traction and stiffness of an adhesive interface with $\mu \geq 1$.
- CCFFM+LEBIM is able to predict the onset of a new finite segment of the crack $\Delta\alpha$ at a given moment. In this way, an abrupt failure of the interface due to adhesive defects can be modelled.

The condition given by (9) corresponds to the CCFFM applied to the LEBIM by the approach based on the stress and energy criteria curves. As an alternative, the PMTE-SC, introduced in [23], can also used to predict the crack onset and/or growth by finite increments of the crack length on a linear elastic interface. This approach seems to more versatile for solving complex fracture problems than the previous methodology. This is mainly because PMTE-SC is more suitable for a general computational implementation of a time stepping procedure covering problems of competition between the initiation and propagation of several cracks. Moreover the total energy can be formulated as a separately convex functional in terms of the displacements and damage variable fields, allowing to apply efficient and robust optimization algorithms to minimize the total energy. According to [23], the PMTE-SC can be formulated by the following constrained minimization

$$\min_{\Delta a \subset A_\sigma} \Delta\Pi(\Delta a) + \Delta R(\Delta a), \tag{10}$$

where, as above, $\Delta\Pi(\Delta a)$ is the increment of the potential energy of the system and $\Delta R(\Delta a)$ the energy dissipated due to a (possibly finite) interface crack advance Δa. For the sake of generality, Δa is understood in (10) as a subset of the interface Γ_C, i.e. $\Delta a \subset \Gamma_C$, possibly being composed by one or several connected components. Δa defines a possible crack advance, representing the set of points on Γ_C that are going to be damaged in this crack advance. $A_\sigma \subset \Gamma_C$ is the subset of all (still) undamaged points on Γ_C where the stress pointwise criterion defined in (3) is satisfied before the considered crack advance happens.

3. Double Cantilever Beam test

The DCB is a well-known test used to determine the fracture energy in pure fracture mode I of adhesively bonded joints. This test allows a good understanding and characterization of the adhesive layer which is very important in the quality evaluation of adhesively bonded joints. In particular it allows determining the parameters that characterize their resistance to fracture and failure. The DCB test is also used to study delamination growth and to compare the performance of different composite laminates. A review of several applications of this test can be found in [28,29].

In Section 3.1, an analytical model is developed to obtain the stress and the displacement fields on the interface between the two beams of the coupon test. Similar models were developed, e.g., in [24,30–33]. With this model, the CCFFM+LEBIM is applied using both the stress and energy criteria curves method and the PMTE-SC. Moreover, the effect of applying displacement or load control is studied, for each of the two approaches of the CCFFM+LEBIM. Both studies will be carried out separately and with an adequate (different) parametrization for each case, in Sections 4 and 5.

One of the most interesting and original result of this work is a detailed study of the PMTE-SC applied to the DCB test. As follows from (10), see also [23], the increment of the potential energy plus the energy dissipated at the abrupt formation of a new debonded part must be equal or smaller than zero,

$$\Delta\Pi(\Delta a) + \Delta R(\Delta a) \leq 0. \tag{11}$$

Let a_0 includes all possible cracks advances previous to the currently studied crack advance Δa. In the first step of specimen analysis, a_0 is given by a possible pre-crack. Then, $a = a_0 + \Delta a$ denotes the current cracked interface part. Then, according to (11), $\Pi(a) + R(a)$ should keep constant or decrease for a new crack onset, $R(a)$ being the total dissipated energy during the fracture of the interface of size a, and $\Pi(a)$ the stored elastic strain energy $U(a)$ plus the potential energy of the external load (negative external work) $\Pi_{ext}(a) = -W(a)$. Therefore, the minimization of the function $\Pi(a) + R(a)$ gives onset of a crack advance Δa associated to the minimum total energy, for a zone Δa of the undamaged interface part which verifies the stress criterion.

Specifically, in this case, the whole interface between the two beams of the DCB is a potential failure zone, starting from a possible initial crack a_0, till the end of the interface. However, the crack growth is only possible in those zones where the stress criterion is satisfied, which will depend on the applied load. The minimization of the function $\Pi(a) + R(a)$ is restricted to these zone. As can be seen in the following sections, there are important differences in the energy behaviour for the DCB test when either load or displacement control is imposed.

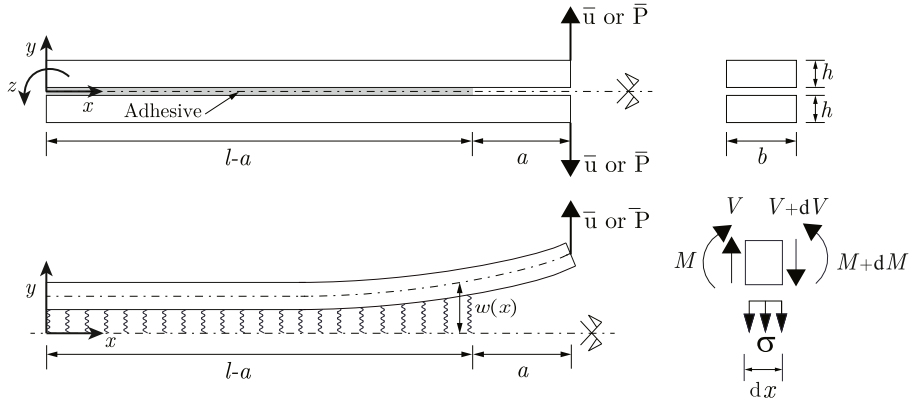

Fig. 2. Double Cantilever Beam test configuration and equilibrium of an infinitesimal element of a beam. The bar over u and P means the imposed boundary conditions.

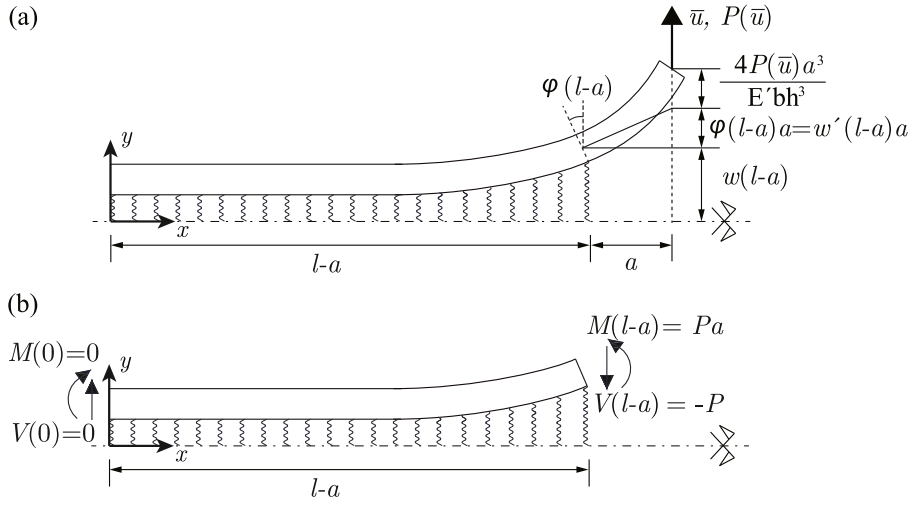

Fig. 3. Boundary conditions used to model the DCB test under displacement control.

In DCB tests the crack growth in mode I is predominant, therefore the interface shear stresses are omitted and the fracture mode mixity angle $\psi(\xi) = 0$.

3.1. Analytical model for the DCB test

Referring to the free-body diagram of an element of length dx represented in Fig. 2, the following equilibrium equations can be written for the upper beam

$$\frac{\mathrm{d}V(x)}{\mathrm{d}x} + b\,\sigma(x) = 0, \tag{12}$$

$$\frac{\mathrm{d}M(x)}{\mathrm{d}x} - V(x) = 0, \tag{13}$$

where $V(x)$ and $M(x)$ are the shear force and the bending moment, and $\sigma(x)$ is the normal stress component on the interface (adhesive layer). The kinematic equations for each of the beams are

$$\chi(x) = \frac{\mathrm{d}\varphi(x)}{\mathrm{d}x}, \tag{14}$$

$$\varphi(x) = \frac{\mathrm{d}w(x)}{\mathrm{d}x}, \tag{15}$$

where $\varphi(x)$, $\chi(x)$ and $w(x)$ are the rotation, curvature and transverse displacement, respectively. The constitutive equation for each beams is

$$\chi(x) = \frac{12M(x)}{E'h^3b}, \tag{16}$$

where, $E' = \frac{E}{(1-\nu^2)}$ is the elastic modulus for plane strain conditions in an isotropic material.

As the adhesive layer is modelled by a spring distribution, then the normal stress component is directly related to the normal relative displacement between the adherents δ_n. Then, the Euler–Bernoulli beam kinematical assumption yields

$$\sigma(x) = k_n\delta_n(x) = 2k_n w(x), \tag{17}$$

where k_n represents the normal stiffness of the adhesive layer, or in a broader view the stiffness of the bonded interface.

By differentiating (15) and accounting for (14) and (16) we obtain

$$\frac{\mathrm{d}^2w(x)}{\mathrm{d}x^2} = \frac{12M(x)}{E'h^3b}. \tag{18}$$

By differentiating (18) we get, in view of (13),

$$\frac{\mathrm{d}^3w(x)}{\mathrm{d}x^3} = \frac{12V(x)}{E'h^3b}. \tag{19}$$

Finally, by differentiating (19), in view of (12) and (17), we get

$$\frac{\mathrm{d}^4w(x)}{\mathrm{d}x^4} + \frac{24k_n w(x)}{E'h^3} = 0. \tag{20}$$

Note that, considering (17) and (20), a similar differential equation for the normal stress component is obtained

$$\frac{\mathrm{d}^4\sigma(x)}{\mathrm{d}x^4} + \frac{24k_n\sigma(x)}{E'h^3} = 0. \tag{21}$$

In order to get dimensionless expressions, the characteristic length parameter l_{ch}, relating the stiffness of the beam to that of the interface,

Table 1
Dimensionless variables and parameters.

$\xi = \frac{x}{l_{ch}}$	$\lambda = \frac{l}{l_{ch}}$	$\alpha = \frac{a}{l_{ch}}$
$\hat{w} = \frac{w}{\bar{u}}$	$\hat{\sigma} = \frac{\sigma}{P/(b\ l_{ch})}$	

is defined in a similar way as in [24,32],

$$l_{ch} = \sqrt[4]{\frac{E' h^3}{6k_n}}. \tag{22}$$

Differential equations (20) and (21) can be rewritten in terms of the dimensionless parameters defined in Table 1 as

$$\hat{w}^{\mathrm{iv}}(\xi) + 4\hat{w}(\xi) = 0, \tag{23}$$

$$\hat{\sigma}^{\mathrm{iv}}(\xi) + 4\hat{\sigma}(\xi) = 0, \tag{24}$$

where the derivatives are now taken with respect to ξ.

Finally, the dimensionless displacement $\hat{w}(\xi)$ and stress $\hat{\sigma}(\xi)$ can be expressed in a similar way as in [24],

$$\hat{w}(\xi) = e^{\xi}(C_1 \sin\xi + C_2 \cos\xi) + e^{-\xi}(C_3 \sin\xi + C_4 \cos\xi), \tag{25}$$

$$\hat{\sigma}(\xi) = e^{\xi}(C_1 \sin\xi + C_2 \cos\xi) + e^{-\xi}(C_3 \sin\xi + C_4 \cos\xi), \tag{26}$$

where $C_1, \ldots, C_4$ are integration constants to be determined from the boundary conditions.

3.2. Displacement solution on the interface under displacement control

The four boundary conditions are obtained by substituting the values of the shear force, bending moment and the displacement at the extreme of the beams into the previous equations. As represented in Fig. 3(b), the first two boundary conditions are given by evaluating (18) and (19) at $x = 0$,

$$\hat{w}''(0) = 0, \tag{27}$$

$$\hat{w}'''(0) = 0. \tag{28}$$

For the third and fourth boundary conditions application it is necessary to write the reaction $P(\bar{u})$ as a function of $w(x)$. According to Fig. 3(b) and (19) the following relation can be obtained

$$w'''(l-a) = \frac{-12P(\bar{u})}{E' h^3 b}. \tag{29}$$

The third boundary condition is shown in Fig. 3(a), where the applied displacement at the extreme of the beams is $\bar{u}$. This displacement is composed of three parts: the normal relative displacement at the crack tip $w(l-a)$, the rotation of the beam at the crack tip by the length of free interface beam a, and the deflection of this free interface beam as a cantilever beam,

$$\bar{u} = w(l-a) + w'(l-a)\ a + \frac{4\ P(\bar{u})\ a^3}{E' h^3 b}. \tag{30}$$

Then, using the relation between $P(\bar{u})$ and $w'''(l-a)$ in (29), the third boundary condition can be written in terms of the dimensionless parameters,

$$\hat{w}(\lambda-\alpha) + \hat{w}'(\lambda-\alpha)\alpha - \hat{w}'''(\lambda-\alpha)\frac{\alpha^3}{3} = 1. \tag{31}$$

Finally, the last boundary condition must satisfy that $M(l-a) = Pa$. Therefore, from (18) and (29) the following boundary condition can be obtained

$$\hat{w}''(\lambda-\alpha) + \hat{w}'''(\lambda-\alpha)\alpha = 0. \tag{32}$$

The system of equations is solved using the computer algebra software Mathematica [34]. The displacement field obtained depends on three of the dimensional parameters defined in the Table 1: ξ, α and λ. However, only ξ and α will change in the rest of the problem formulation, since ξ refers to any point on the interface between the beams and α refers to the crack tip location. Recall that α_0 includes all possible cracks advances previous to the currently studied crack advance $\Delta\alpha$, and $\alpha = \alpha_0 + \Delta\alpha$. Therefore, in the rest of the formulation, the displacement field is written in terms of the two variables ξ and α. Thus, (33) represents the solution of the displacement field on the interface for any undamaged point ξ and a crack length α,

$$\begin{aligned}
\hat{w}(\xi,\alpha) = \Big[& -3\left(e^{3\alpha+\zeta+\lambda} + e^{\alpha-\zeta+3\lambda}\right)\alpha\cos(\alpha-\zeta-\lambda) \\
& + 3\,e^{3\alpha-\zeta+\lambda}\left(\left(-1-e^{2\zeta}+\alpha\right)\cos(\alpha+\zeta-\lambda)\right) \\
& - 3\,e^{3\alpha-\zeta+\lambda}\left(e^{2\zeta}\left(-1+\alpha\right)\sin(\alpha-\zeta-\lambda)\right) \\
& - 3\,e^{3\alpha-\zeta+\lambda}\left(\left(\alpha+e^{2\zeta}(-1+2\alpha)\right)\sin(\alpha+\zeta-\lambda)\right) \\
& + 3\,e^{\alpha-\zeta+3\lambda}\left(\left(1+e^{2\zeta}(1+\alpha)\right)\cos(\alpha+\zeta-\lambda)\right) \\
& + 3\,e^{\alpha-\zeta+3\lambda}\left(2\cos(\zeta)\sin(\alpha-\lambda)\right) \\
& + 3\,e^{\alpha-\zeta+3\lambda}\,\alpha\left(\sin(\alpha-\zeta-\lambda) + (2+e^{2\zeta})\sin(\alpha+\zeta-\lambda)\right)\Big] \Big/ \\
& \Big[e^{4\alpha}\left(-3+2\alpha\left(3+(-3+\alpha)\alpha\right)\right) \\
& + e^{4\lambda}\left(3+2\alpha\left(3+\alpha(3+\alpha)\right)\right) \\
& + 2\,e^{2(\alpha+\lambda)}\left(-4\alpha^3+2\alpha\left(-3+\alpha^2\right)\cos\left(2(\alpha-\lambda)\right)\right) \\
& + 2\,e^{2(\alpha+\lambda)}\left(\left(3-6\alpha^2\right)\sin\left(2(\alpha-\lambda)\right)\right)\Big].
\end{aligned} \tag{33}$$

The displacement at the crack tip, necessary for the rest of the problem development, is obtained by evaluating the previous expression for $\xi = \lambda - \alpha$,

$$\begin{aligned}
\hat{w}(\lambda-\alpha,\alpha) = \Big[& 3\,e^{4\alpha}(-1+\alpha) + 3\,e^{4\lambda}(1+\alpha) \\
& - 6\,e^{2(\alpha+\lambda)}\left(\alpha\cos\left(2(\alpha-\lambda)\right) - \sin\left(2(\alpha-\lambda)\right)\right)\Big] \Big/ \\
& \Big[e^{4\alpha}\left(-3+2\alpha\left(3+(-3+\alpha)\alpha\right)\right) \\
& + e^{4\lambda}\left(3+2\alpha\left(3+\alpha(3+\alpha)\right)\right) \\
& + 2\,e^{2(\alpha+\lambda)}\left(-4\alpha^3+2\alpha\left(-3+\alpha^2\right)\cos\left(2(\alpha-\lambda)\right)\right) \\
& + 2\,e^{2(\alpha+\lambda)}\left(\left(3-6\alpha^2\right)\sin\left(2(\alpha-\lambda)\right)\right)\Big].
\end{aligned} \tag{34}$$

3.3. Stress solution on the interface under load control

The four boundary conditions are obtained by substituting the values of the shear force and the bending moment at $x = 0$ and $x = l-a$, as shown in Fig. 4(b).

Thus, the first two boundary conditions are given by evaluating (18) and (19) at $x = 0$. These boundary conditions can be expressed in terms of the normal stress component, see (17),

$$\hat{\sigma}''(0) = 0, \tag{35}$$

$$\hat{\sigma}'''(0) = 0. \tag{36}$$

In the third boundary condition, $V(l-a) = -\bar{P}$ must be fulfilled, and from (19) the following expression can be obtained

$$\hat{\sigma}'''(\lambda-\alpha) = -4. \tag{37}$$

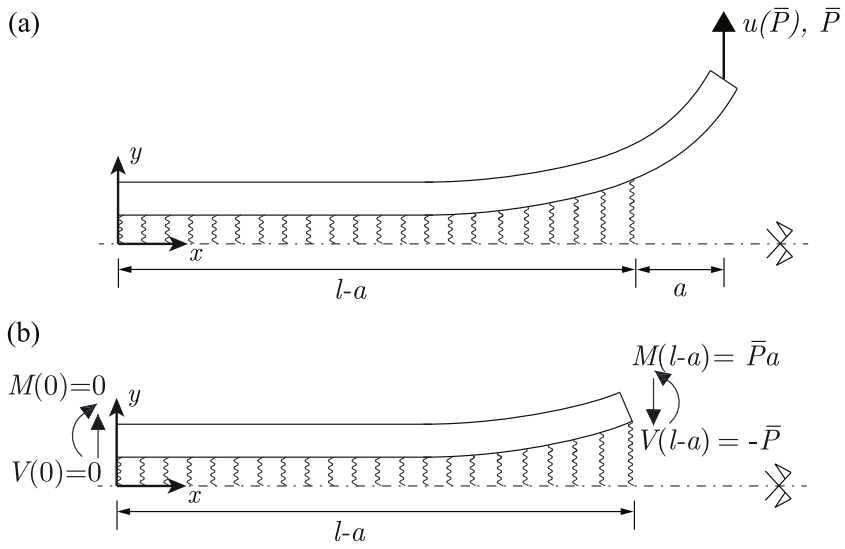

Fig. 4. Boundary conditions used to model the DCB test under load.

The last boundary condition is obtained from (18) to satisfy $M(l-a) = \bar{P}a$,

$$\hat{\sigma}''(\lambda-\alpha) = 4\alpha. \tag{38}$$

In a similar way as done for the analysis under displacement control, this system is solved by using Mathematica. Then, the stress distribution on the interface is obtained, it depends on the same parameters and variables as the solution defined in Section 3.3. Thus, the following function defines the normal stress component at a point ξ within an undamaged zone of the interface, and a crack length α,

$$\begin{aligned}\hat{\sigma}(\xi,\alpha) = \Big[& -2\left(e^{3\alpha+\zeta+\lambda}+e^{\alpha-\zeta+3\lambda}\right)\alpha\cos(\alpha-\zeta-\lambda)\\ & +2e^{3\alpha-\zeta+\lambda}\left(\left(-1-e^{2\zeta}+\alpha\right)\cos(\alpha+\zeta-\lambda)\right)\\ & -2e^{3\alpha-\zeta+\lambda}\left(e^{2\zeta}\left(-1+\alpha\right)\sin(\alpha-\zeta-\lambda)\right)\\ & -2e^{3\alpha-\zeta+\lambda}\left(\left(\alpha+e^{2\zeta}(-1+2\alpha)\right)\sin(\alpha+\zeta-\lambda)\right)\\ & +2e^{\alpha-\zeta+3\lambda}\left(\left(1+e^{2\zeta}(1+\alpha)\right)\cos(\alpha+\zeta-\lambda)\right)\\ & +2e^{\alpha-\zeta+3\lambda}\left(2\cos(\zeta)\sin(\alpha-\lambda)\right)\\ & +2e^{\alpha-\zeta+3\lambda}\alpha\left(\sin(\alpha-\zeta-\lambda)+(2+e^{2\zeta})\sin(\alpha+\zeta-\lambda)\right)\Big] \Big/\\ & \left[e^{4\alpha}+e^{4\lambda}+2e^{2(\alpha+\lambda)}\left(-2+\cos\left(2(\alpha-\lambda)\right)\right)\right].\end{aligned} \tag{39}$$

Note that, although (39) seems to be different from (33), the two equations are equivalent but associated to different dimensionless parameters. This can be clearly seen from (29), since this equation defines the relationship between the $\bar{u}$ under displacement control and $\bar{P}$ under load control, i.e., for an imposed displacement $\bar{u}$, the reaction of the system at the same point would be $P = -\bar{u}\,\frac{k_n l_{ch} b}{2}\hat{w}'''(\lambda-\alpha)$, and vice versa. Therefore, the relationships between $\hat{w}$ and $\hat{\sigma}$ is $4\hat{w} = \hat{w}'''(\lambda-\alpha)\,\hat{\sigma}$ for a specific $\bar{u}$ with the associated specific $\bar{P}$.

Table 2
Default mechanical and geometrical characteristics used for the debond analysis of the DCB test.

	l (mm)	h (mm)	a_0 (mm)	E (GPa)	ν
Beams	237	1.5	0	135	0.3
	k_n (MPa/μm)				
Adhesive	0.30				
Characteristic length:	l_{ch} = 4.08388 mm				
Dimensionless parameter:	λ = 58.033				

The normal stress at the crack tip under load control is obtained by evaluating the expression in (39) for $\xi = \lambda - \alpha$,

$$\begin{aligned}\hat{\sigma}(\lambda-\alpha,\alpha) = \Big[& 2e^{4\alpha}(-1+\alpha)+2e^{4\lambda}(1+\alpha)\\ & -4e^{2(\alpha+\lambda)}\left(\alpha\cos\left(2(\alpha-\lambda)\right)-\sin\left(2(\alpha-\lambda)\right)\right)\Big] \Big/\\ & \left[e^{4\alpha}+e^{4\lambda}+2e^{2(\alpha+\lambda)}\left(-2+\cos\left(2(\alpha-\lambda)\right)\right)\right].\end{aligned} \tag{40}$$

However, this equation is different from that for the displacement at the crack tip under displacement control, see (34). This is due to the fact that this function represents the evolution of the stress in the crack tip with the crack size α and for a specific $\bar{P}$. Recall that α includes all possible previous crack advances and the current crack advance, i.e. $\alpha = \alpha_0 + \Delta\alpha$. Further explanations are included in the next section with an example for clarification.

3.4. Stress and displacement distributions on the interface for a specific case

In order to analyse the behaviour of the stress and displacement solutions at the crack tip obtained in the previous sections, the data included in Table 2 are used to graphically represent them for a specific interface. The obtained values of the dimensionless parameters defined in Table 1 are also presented in Table 2.

Note that the dimensionless equations developed in this article are independent of the fracture energy and the critical stress. This is because these mechanical properties are used to define the dimensionless solution of the problem. Moreover, the width of the beam does not influence the stress distributions and relative displacement field along the interface. Additionally, as this is a purely theoretical study, whose

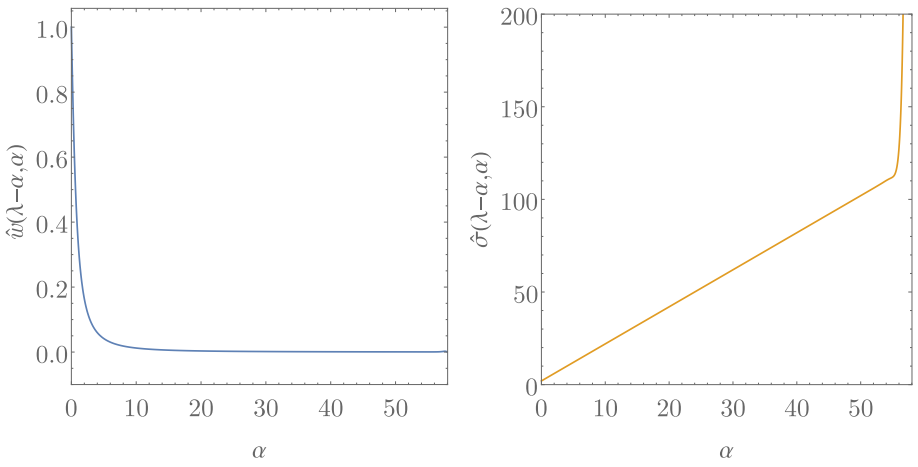

(a) $\hat{w}(\lambda-\alpha,\alpha)$ (b) $\hat{\sigma}(\lambda-\alpha,\alpha)$

Fig. 5. Crack tip value of $\hat{w}(\lambda-\alpha,\alpha)$ under displacement control and $\hat{\sigma}(\lambda-\alpha,\alpha)$ under load control, from $\alpha=\alpha_0=0$ to $\alpha=\lambda$.

aim is to analyse the CCFFM, it is considered appropriate to start the test without a pre-crack, i.e. $a_0=0$.

Fig. 5(a) represents the solution obtained by (34), where the dimensionless displacement at the crack tip is obtained as a function of the dimensionless crack length from $\alpha=\alpha_0=0$ to $\alpha=\lambda$ under displacement control. It can be seen that the displacement at the crack tip decreases when the crack length increases. Fig. 5(b) represents the solution obtained by (40), where the dimensionless stress at the crack tip is obtained as a function of the dimensionless crack length from $\alpha=\alpha_0=0$ to $\alpha=\lambda$ under load control. It can be seen that the stress at the crack tip increases when the crack length increases.

As follows from Fig. 5, the evolution of both solutions is very different for load and displacement control. These different behaviours of the two solutions will result in a significant difference in the evolution of the interface failure for each configuration.

4. CCFFM applied to a linear-elastic interface for the DCB under displacement control

4.1. Solution obtained by the stress and energy criteria curves

Based on the theoretical concepts exposed in [17,19,21], for the specific case of the DCB test under displacement control, the ERR can be defined for a point associated with the crack tip, whose position in this system is $\lambda-\alpha'$, as

$$G(a')=2k_n\bar{u}^2\hat{w}^2(\lambda-\alpha',\alpha')=2k_n\bar{u}^2\hat{G}(\lambda-\alpha') \quad \text{with} \quad \hat{G}(\lambda-\alpha')=\hat{w}^2(\lambda-\alpha',\alpha') \tag{41}$$

where α', with $a'=\alpha' l_{ch}$, represents the "virtual advance" of the crack tip, between α_0 and α, in the energy criterion framework. The initial crack length a_0 includes all possible cracks advances previous to the currently studied crack advance $\Delta\alpha$, and $\alpha=\alpha_0+\Delta\alpha$.

Therefore, to initiate or propagate an interface crack by a finite increment of its length, the following energy balance condition, based on (5), must be fulfilled:

$$\frac{2k_n\bar{u}^2}{G_{\mathrm{Ic}}}\geq g(\Delta\alpha) \quad \text{with} \quad g(\Delta\alpha)=\frac{\Delta\hat{R}(\Delta\alpha)}{-\Delta\hat{\Pi}(\Delta\alpha)}=\frac{\Delta\alpha}{\int_{\alpha_0}^{\alpha_0+\Delta\alpha}\hat{G}(\lambda-\alpha')\,\mathrm{d}\alpha'}, \tag{42}$$

where in general the dimensionless $g(\Delta\alpha)$, defined by (6), is the quotient of the dimensionless dissipated energy $\Delta\hat{R}(\Delta\alpha)$ and the dimensionless energy released (the decrease of the dimensionless potential energy $\Delta\hat{\Pi}(\Delta\alpha)$ by this (typically instantaneous) finite crack-advance. Actually, in the present case of pure mode I crack advance, $g(\Delta\alpha)$ is the reciprocal of the average of the dimensionless ERR on a finite segment given by the finite crack-advance.

In order to be consistent with the nondimensionalisation used in the previous sections and to be able to subsequently compare both results obtained under displacement and load control, the definition of critical displacement as

$$w_{\mathrm{c}}=\frac{\delta_{\mathrm{c}}}{2}=\frac{\sigma_{\mathrm{c}}}{2k_n} \tag{43}$$

is used, where σ_{c} and δ_{c} are the critical normal stress and the relative displacement between the beams of the specimen associated to pure mode I and represented in Fig. 1.

The stress criterion is evaluated, based on (3), along the undamaged interface and must be satisfied in the same $\Delta\alpha$ zone as the energy criterion, i.e. $\lambda-\alpha_0-\Delta\alpha\leq\xi\leq\lambda-\alpha_0$, for a given value of α_0,

$$\frac{\bar{u}}{w_{\mathrm{c}}}\geq s(\xi)=\frac{1}{\hat{w}(\xi,\alpha_0)} \quad \text{for all } \xi,\ \lambda-\alpha_0-\Delta\alpha\leq\xi\leq\lambda-\alpha_0. \tag{44}$$

Nevertheless, as $s(\xi)$ increases with decreasing ξ, the above stress criterion condition can be written just for the minimum value of ξ considered, i.e., $\frac{\bar{u}}{w_{\mathrm{c}}}\geq s(\lambda-\alpha_0-\Delta\alpha)$. For the sake of simplicity, the following convention will be assumed: $s(\Delta\alpha)\overset{\mathrm{def}}{=}s(\lambda-\alpha_0-\Delta\alpha)$.

Finally, the parameter μ in (7), defined tacitly for typical load control, is redefined here to be suitable for displacement control, writing it in terms of the critical displacement (without changing the value of μ), as

$$\mu=\frac{G_{\mathrm{Ic}}}{2k_n w_{\mathrm{c}}^2}. \tag{45}$$

The CCFFM given by the stress and energy criteria curves can be expressed as

$$\frac{\bar{u}}{w_{\mathrm{c}}}\geq\frac{\bar{u}_{\mathrm{f}}}{w_{\mathrm{c}}}=\min_{\Delta\alpha}\max\left\{s(\Delta\alpha),\sqrt{\mu\ g(\Delta\alpha)}\right\}, \tag{46}$$

where $\bar{u}_{\mathrm{f}}$ is the minimum displacement applied at the beam end that satisfies both criteria and produces a crack advance by length $\Delta\alpha_{\mathrm{c}}=\Delta\alpha$.

In order to interpret the behaviour of the failure criterion in (46) for this specific test, the two criteria curves are plotted in Fig. 6 using the geometrical and mechanical characteristics described in Table 2, for $\mu=8$.

Fig. 6 shows that for small values of $\Delta\alpha$, the energy criterion curve (represented by the yellow line) starts above the stress criterion curve (represented by the blue line), both having a positive slope. Actually, the initial part of the energy criterion function, for $\Delta\alpha\to 0$, always gives larger values than those obtained in the initial part of the stress

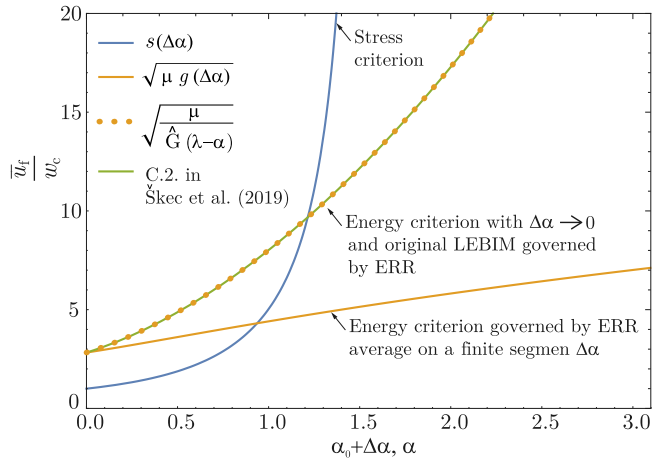

Fig. 6. Functions associated to the energy criterion, $\sqrt{\mu g(\Delta\alpha)}$ and $\sqrt{\frac{\mu}{\hat{G}(\lambda-\alpha)}}$, and function of the stress criterion $s(\Delta\alpha)$, using the geometrical and mechanical characteristics described in Table 2, for $\mu = 8$ and $\alpha_0 = 0$.

criterion function, due to $\mu > 1$. However, the shape of the increasing function $\sqrt{\mu\ g(\Delta\alpha)}$ depends on the problem type. If the slope of the energy criterion curve increases continuously until the intersection with the stress criterion curve, the growth of the interface crack will be infinitesimal with $\Delta\alpha_c \to 0$. This leads to a stable crack propagation, i.e. if the displacement at the ends of the beams is continuously increased, the interface debond growth is also produced in a continuous way with $\alpha = \alpha_0 + d\alpha$. Consequently, in this occasion, as in the original LEBIM, the interface failure is in fact only governed by the ERR, instead of the ERR average on a finite segment, and the failure criterion (46) can be expressed as

$$\frac{\bar{u}}{w_c} \geq \frac{\bar{u}_f}{w_c} = \sqrt{\frac{\mu}{\hat{G}(\lambda-\alpha)}}. \tag{47}$$

Notice that the expression under the square root in the above criterion is the limit of $\mu\ g(\Delta\alpha)$ for $\Delta\alpha \to 0$, i.e. recovering the prediction by the original LEBIM but with the critical energy given by $G_{Ic} = \mu\ 2k_n w_c^2$ according to (45).

In Fig. 6, the CCFFM + LEBIM solution for this test is shown as a dashed yellow line. To verify the solution obtained with this method, the results have been compared with the solution obtained in [33] (green line). Equation C.2 in [33] shows the load required for crack initiation and propagation, for a solution of the Euler–Bernoulli beam theory for a DCB with a linear-elastic interface with brittle failure.

4.2. Solution obtained by the PMTE-SC

The change in the potential energy of a system $\Delta\Pi$ is given by the change of the strain energy ΔU and the work of external forces ΔW, i.e. $\Delta\Pi = \Delta U - \Delta W$. Recall that ΔW vanishes under displacement control. Thus, the incremental energy balance (11) for this test under displacement control can be expressed as

$$\Delta U(\Delta a) + \Delta R(\Delta a) \leq 0. \tag{48}$$

Therefore, in this case the total energy function $U(a) + R(a)$ is minimized subjected to a stress condition. In the following section, the energy formulation used to obtain $U(a) + R(a)$ is explained, and the calculation of its minimum by the definition of the ERR, for this specific case, is shown. Eventually, the PMTE-SC is applied to the same test studied previously by the CCFFM+LEBIM, applying the stress and energy criteria curves, in Section 4.1.

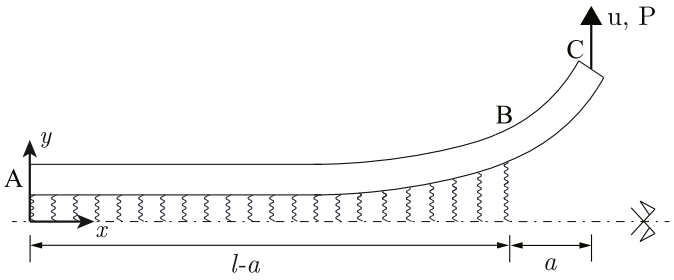

Fig. 7. DCB test configuration.

4.2.1. Energy based formulation

For an easier understanding of the present formulation, the zone of the beam including an undamaged interface is named AB, and the zone of the beam where the interface is damaged is called BC, as shown in Fig. 7. In general, the strain energy of both zones according to the Euler–Bernoulli theory can be expressed as

$$\begin{aligned} U_{AB} &= 2U_{AB\ beam} + 2U_{AB\ interface}, \\ U_{BC} &= 2U_{BC\ beam}, \end{aligned} \tag{49}$$

where,

$$\begin{aligned} U_{AB\ beam} &= \int_{AB} \frac{1}{2}\left(\frac{12M(x)^2}{E'h^3 b}\right) dx, \\ U_{AB\ interface} &= \int_{AB} \frac{1}{2}\ b\ \sigma(x)w(x)dx, \\ U_{BC\ beam} &= \int_{BC} \frac{1}{2}\left(\frac{12M(x)^2}{E'h^3 b}\right) dx. \end{aligned} \tag{50}$$

Relations (50) show that the strain energy of a beam is the sum of the strain energies corresponding to the internal work within the beam and that corresponding to the interface springs. Notice that, as this model is based on the Euler–Bernoulli beam theory, the shear strain energy has not been taken into account, because the shear deformation of the beam is neglected. It should also be noticed that the displacements on the interface $w(x)$ is half of $\delta_n(x)$, the relative normal displacement between the two beams. The solution for $w(x)$ in AB zone is given by (33), it depends on two problem variables a and x, and is written in dimensionless form as $\hat{w}(\xi,\alpha)$. Remember that $\alpha = \alpha_0 + \Delta\alpha$ includes also all possible cracks advances previous to the currently studied crack advance $\Delta\alpha$. The energy expressions in this section are presented for a specific configuration of the DCB with a debonded zone α and a bonded zone $\lambda - \alpha$. The dependence on these two variables must be taken into account in order to calculate the definite integrals included in (50).

In view of (50) and substituting the equations of the beam moment (18) and the stresses on the interface (17), the dimensionless elastic energy at AB zone can be written as

$$\hat{U}_{AB}(\alpha) = \frac{12\ l_{ch}^3}{E'h^3\ b\ \bar{u}^2} U_{AB}(a) = \int_0^{\lambda-\alpha} \left(\frac{\partial^2 \hat{w}(\xi,\alpha)}{\partial\xi^2}\right)^2 + 4\left(\hat{w}(\xi,\alpha)\right)^2 d\xi, \tag{51}$$

where the first term of the integral is associated with the deformation of the two beams and the second term is associated with the deformation of the interface.

For the determination of the elastic energy of the BC zone, the equations of the free-body diagram developed in Section 3.1 cannot be used, because these are formulated only for the zone where an elastic interface exists. However, the bending moment equation in BC zone can be easily deduced, as

$$M(x) = P(l-x) \quad \text{for all} \quad x,\ l-a \leq x \leq l. \tag{52}$$

Taking into account the relationship between the load at the beam ends and the vertical displacement of the crack tip by (29), the elastic energy

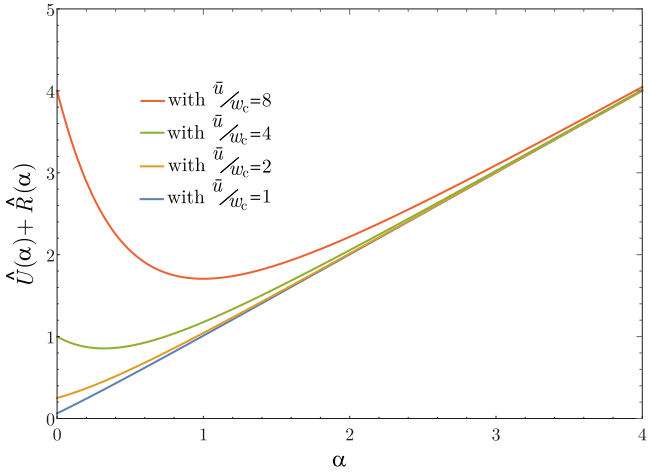

Fig. 8. Total energy function $\hat{U}(\alpha)+\hat{R}(\alpha)$ for several values of the dimensionless boundary condition in displacement $\frac{\bar{u}}{w_c}$, for $\mu = 8$.

of BC zone can be expressed as

$$\hat{U}_{BC}(\alpha) = \frac{12\ l_{ch}^3}{E' h^3\ b\ \bar{u}^2} U_{BC}(a) = \int_{\lambda-\alpha}^{\lambda} \left((\lambda-\xi) \frac{\partial^3 \hat{w}(\lambda-\alpha,\alpha)}{\partial \xi^3} \right)^2 d\xi. \tag{53}$$

The energy dissipated by the abrupt formation of a new crack and the total dissipated energy including the formation of the new debond on the interface are given by the fracture energy in Mode I

$$R(\Delta a) = G_{Ic} \Delta a\, b \quad \text{and} \quad R(a) = G_{Ic} a\, b. \tag{54}$$

Finally, the total energy function to be minimized can be expressed as

$$\begin{aligned} U(a)+R(a) &= \frac{E' h^3\ b\ \bar{u}^2}{12\ l_{ch}^3} \left(\hat{U}_{AB}(\alpha) + \hat{U}_{BC}(\alpha) \right) + b\ l_{ch} G_{Ic} \alpha \\ &= b\ l_{ch} G_{Ic} \left(\frac{\bar{u}^2}{4\mu w_c^2} \left(\hat{U}_{AB}(\alpha) + \hat{U}_{BC}(\alpha) \right) + \alpha \right), \end{aligned} \tag{55}$$

and in dimensionless form as

$$\hat{U}(\alpha)+\hat{R}(\alpha) = (U(a)+R(a)) \frac{1}{b\ l_{ch} G_{Ic}} = \frac{\bar{u}^2}{4\mu w_c^2} \left(\hat{U}_{AB}(\alpha) + \hat{U}_{BC}(\alpha) \right) + \alpha. \tag{56}$$

The graphs of the total energy function shown in Fig. 8 are obtained using (56) and the parameters included in Table 2, for $\mu = 8$ and for several displacement values imposed at the beam ends. Results in Fig. 8 show that for small values of the imposed displacement $\frac{\bar{u}}{w_c}$, the minimum of the function is obtained at $\alpha = 0$, i.e. no crack growth. However, when the imposed displacement increases, the total energy function becomes steeply convex with a minimum for values of $\alpha > 0$. Recall that the calculation of the energies is for a specific configuration of the problem with a certain debonded zone of the interface $\alpha = \alpha_0 + \Delta\alpha$. It should be noted that if the problem had an initial pre-crack length, e.g., $\alpha_0 = 2$, none of the four imposed displacements represented in Fig. 8 would cause an interface failure. This is because none of the total energy functions have their minimum for $\alpha > 2$.

A way to find the local minimum of the total energy functions obtained by (56), is to use the first-derivative test within the interval for α where the stress criterion is fulfilled,

$$\frac{d\hat{U}(\alpha)}{d\alpha} + \frac{d\hat{R}(\alpha)}{d\alpha} = 0. \tag{57}$$

The expression of the ERR in (41) is used to calculate the first term of the derivative, as in LEFM the ERR G is given by the negative variation of the potential energy per unit area of the crack. However, as mentioned above, under displacement control the potential energy equals the elastic strain energy, thus

$$G(a) = -\frac{d\Pi(a)}{b\ da} = -\frac{dU(a)}{b\ da} \tag{58}$$

The ERR at the crack tip with $\xi = \lambda - \alpha$ is defined in (41) but replacing α' by α. While the derivative of the elastic strain energy of the whole system with respect to the crack length α can be obtained using (51) and (53),

$$\begin{aligned} \frac{dU(a)}{b da} &= \frac{E' h^3 \bar{u}^2}{12 l_{ch}^4} \left(\frac{d\hat{U}_{AB}(\alpha)}{d\alpha} + \frac{d\hat{U}_{BC}(\alpha)}{d\alpha} \right) \\ &= \frac{\bar{u}^2 k_n}{2} \left(\frac{d\hat{U}_{AB}(\alpha)}{d\alpha} + \frac{d\hat{U}_{BC}(\alpha)}{d\alpha} \right). \end{aligned} \tag{59}$$

Therefore, the relationship between the expressions of the ERR and the derivative of the elastic strain energy, in dimensionless form, becomes

$$4\hat{G}(\lambda-\alpha) = 4\left(\hat{w}(\lambda-\alpha,\alpha)\right)^2 = -\left(\frac{d\hat{U}_{AB}(\alpha)}{d\alpha} + \frac{d\hat{U}_{BC}(\alpha)}{d\alpha} \right). \tag{60}$$

Hence, the local extreme point of the total energy function is produced for an α value which satisfies

$$\frac{dU(a)}{b da} + \frac{dR(a)}{b da} = -2k_n \bar{u}^2 (\hat{w}(\lambda-\alpha,\alpha))^2 + G_{Ic} = 0, \tag{61}$$

and substituting G_{Ic} from (45), the dimensionless expression of (61) is obtained

$$\frac{\bar{u}}{w_c} \left(\hat{w}(\lambda-\alpha,\alpha) \right) = \sqrt{\mu}. \tag{62}$$

Fig. 9 represents the dimensionless total energy given by (56), for the data included in Table 2 and $\mu = 8$, and for several values of the two input variables: the displacement imposed at the beam ends $\frac{\bar{u}}{w_c}$ and the damaged interface length α. The convex total energy function defines a surface where the "warm" colours represent the areas of the surface with the lowest energy, and "cold" colours the areas with the highest energy. The red dots located in the surface valley are the minimum values for each displacement imposed $\frac{\bar{u}}{w_c}$ obtained using (62).

4.2.2. Application of the PMTE-SC to a specific case and comparison between methods

Fig. 10 shows the function $\hat{U}(\alpha)+\hat{R}(\alpha)$ for the geometrical and mechanical characteristics described in Table 2 and $\mu = 8$. As an example and in order to describe the total energy behaviour, eleven different $\frac{\bar{u}}{w_c}$ values are used, which represent the displacement imposed at the beam ends for the same w_c. These displacements are increased from 1 to 3.03, in intervals of 0.203 (this value is chosen so the initial part of one of the curves coincides with the initial part of the energy criterion curve, see Fig. 6, and to get a reasonable size of the displacement increment). Fig. 10 shows that for increasing values of $\frac{\bar{u}}{w_c}$ the initial values of these curves (for $\alpha_0 = 0$) and their curvatures increase.

Before looking for the minimum of each represented function, the interface zone that verifies the stress criterion must be analysed in each curve, because the minimum of the function is looked for only within this zone. The interface zone that fulfils the stress criterion (44) can be obtained for each ξ point on the undamaged interface part,

Stress criterion (44) defines the zone including points (ξ values) which are prone to fail by the imposed displacement $\bar{u}$. This zone is represented in Fig. 10 by a dashed line in each curve. For increasing $\frac{\bar{u}}{w_c}$ the zone satisfying the stress criterion also increases, starting from the first curve, where no point verifies (44), to the last curve, which has the largest zone where failure is possible. Once the zone where interface failure is possible according to the stress criterion is computed, the minimum of the total energy $\hat{U}(\alpha)+\hat{R}(\alpha)$ is determined by means of the ERR, as described in the previous section. However, from the eleven curves plotted in Fig. 10, only the last two (those produced by the largest $\frac{\bar{u}}{w_c}$) satisfy the condition (62) for an α which verifies the stress criterion. The minima of these last two curves are represented in the figure by filled circles. Note that, the minimum $\frac{\bar{u}}{w_c}$ that has to be applied to initiate crack growth, corresponds to the green curve with the imposed displacement $2\sqrt{2}$, since the derivative of this curve

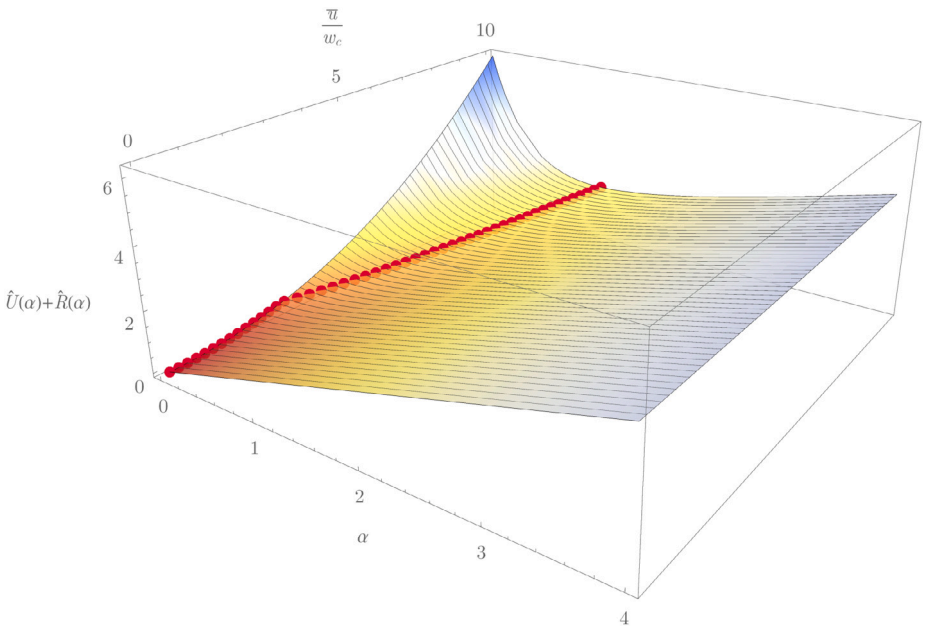

Fig. 9. Dimensionless total-energy surface given by (56), and the minimum values for each load and for the data included in Table 2 and $\mu = 8$.

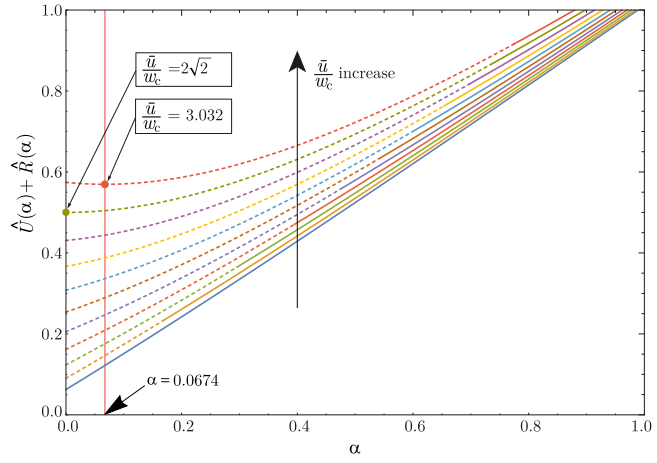

Fig. 10. Dimensionless total energy $\hat{U}(\alpha)+\hat{R}(\alpha)$ for several values of the dimensionless imposed displacement $\frac{\bar{u}}{w_c}$ (ranging from 1 to 3.03 in intervals of 0.203). The discontinuous lines indicate the intervals of α values that satisfy the stress criterion. The filled circles represent the minimum of the curves that satisfies the condition (62).

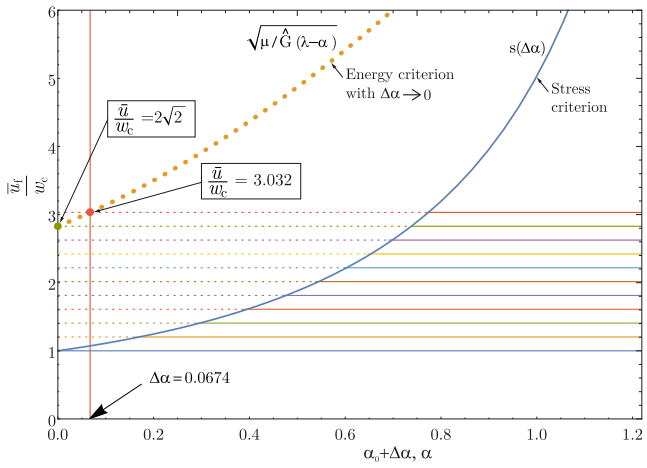

Fig. 11. Comparison of the $\Delta\alpha$ value predicted using PMTE-SC and the stress and energy criteria curves methodology. Each horizontal line represents the same applied dimensionless displacement $\frac{\bar{u}}{w_c}$ included in Fig. 10.

vanishes at $\alpha = 0$. For example, the last (red) curve with $\frac{\bar{u}}{w_c} = 3.03$ produces a crack growth up to $\alpha = 0.0674$. The rest of the curves of the total energy, with $\frac{\bar{u}}{w_c} < 2\sqrt{2}$, start with a positive slope at $\alpha = 0$, thus, they do not satisfy the energy balance condition to initiate crack growth, although the stress criterion allows crack initiation in these cases as well.

For a deeper understanding of the PMTE-SC methodology, the results in Fig. 10 are compared with the results obtained by the CCFFM+LEBIM using the stress and energy criteria curves, developed in Section 4.1. Fig. 11 shows the curves $s(\Delta\alpha)$ and $\sqrt{\frac{\mu}{\hat{G}(\lambda-\alpha)}}$ for $\mu = 8$, obtained in Section 4.1. For comparison purposes, horizontal lines coinciding with $\frac{\bar{u}}{w_c}$ values and colours used in Fig. 10 are also included in the plot. In Fig. 11 the intersection of the horizontal lines with the $s(\Delta\alpha)$ curve is indicated by the change from dashed to continuous lines. The dashed parts of these lines represent, for each $\frac{\bar{u}}{w_c}$, the length of the zone $\Delta\alpha$ where the damage is allowed according to the stress criterion. Notice that these zones coincide with those indicated by the associated dashed lines in Fig. 10. Moreover, according to the stress and energy criteria curves, $\frac{\bar{u}}{w_c} = 2\sqrt{2}$ is the minimum applied displacement that initiates the interface damage, and $\frac{\bar{u}}{w_c} = 3.03$ is the applied displacement shown in the figure producing the interface crack propagation with $\Delta\alpha = 0.0674$ (recall that the crack growth predicted is infinitesimal), exactly as predicted by the PMTE-SC approach.

5. CCFFM applied to a linear-elastic interface for the DCB under load control

5.1. Solution obtained by the stress and energy criteria curves

Following the previous case, for the specific case of the DCB test under load control, the ERR can be expressed as

$$G(a') = \frac{\bar{P}^2}{b^2 l_{ch}^2 2k_n}\hat{\sigma}^2(\lambda-\alpha',\alpha') = \frac{\bar{P}^2}{b^2 l_{ch}^2 2k_n}\hat{G}(\lambda-\alpha') \quad \text{with} \quad \hat{G}(\lambda-\alpha') = \hat{\sigma}^2(\lambda-\alpha',\alpha'). \tag{63}$$

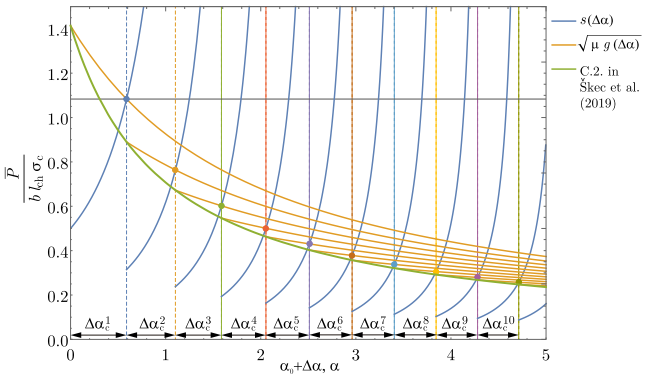

Fig. 12. Stress and energy criteria functions $s(\Delta\alpha)$ (blue lines) and $\sqrt{\mu g(\Delta\alpha)}$ (yellow lines), for the DCB under load control with $\mu = 8$, and several load steps.

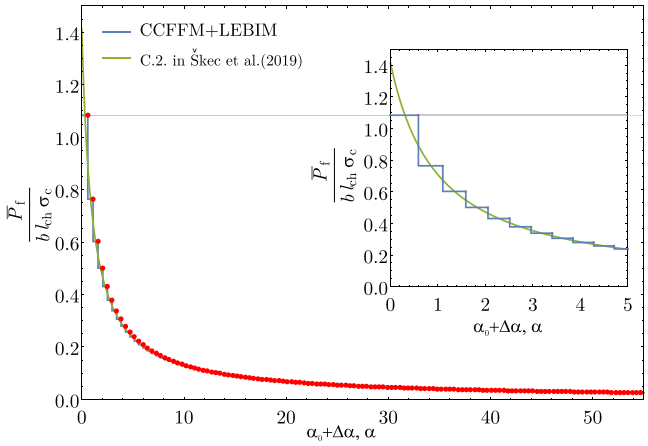

Fig. 13. Load — Crack propagation curve for the DCB test under load control.

Remember that α' represents the "virtual advance" of the crack tip in the energy criterion framework.

Following the above relations, the energy criterion, based on (5), can be written as

$$\frac{\bar{P}^2}{b^2 l_{ch}^2 2k_n G_{Ic}} \geq g(\Delta\alpha) \quad \text{with} \quad g(\Delta\alpha) = \frac{\Delta\hat{R}(\Delta\alpha)}{-\Delta\hat{\Pi}(\Delta\alpha)} = \frac{\Delta\alpha}{\int_{\alpha_0}^{\alpha_0+\Delta\alpha} \hat{G}(\lambda-\alpha')\,\mathrm{d}\alpha'}. \tag{64}$$

As in the previous section, the stress criterion, based on (3), depends on σ_c and can be expressed as a function of ξ, for a specific value of α_0,

$$\frac{\bar{P}}{b\, l_{ch}\sigma_c} \geq s(\xi) = \frac{1}{\hat{\sigma}(\xi,\alpha_0)} \quad \text{for all } \xi,\ \lambda-\alpha_0-\Delta\alpha \leq \xi \leq \lambda-\alpha_0. \tag{65}$$

For the sake of simplicity, the following convention will be assumed also here: $s(\Delta\alpha) \overset{\text{def}}{=} s(\lambda-\alpha_0-\Delta\alpha)$.

Finally, using the parameter μ defined in (7), the CCFFM by can be defined as:

$$\frac{\bar{P}}{b\, l_{ch}\sigma_c} \geq \frac{\bar{P}_f}{b\, l_{ch}\sigma_c} = \min_{\Delta\alpha} \max \left\{ s(\Delta\alpha), \sqrt{\mu\ g(\Delta\alpha)} \right\}, \tag{66}$$

where $\bar{P}_f$ is the minimum load applied to the beam end that satisfies both criteria and produces a crack advance with length $\Delta\alpha = \Delta\alpha_c$. Fig. 12 shows the stress and energy criteria functions in (66), for the geometrical and mechanical characteristics described in Table 2 and $\mu = 8$. These functions are plotted for several load steps, given by different lengths of the initial crack α_0 in each step.

Unlike the previous configuration under displacement control, the energy criterion starts with a negative slope, above the stress criterion. Therefore, the minimum load that satisfies both criteria is given by the intersection of the curves. This produces an instantaneous onset of a new finite segment of the crack $\Delta\alpha_c$ for a specific load $\frac{\bar{P}_f}{b\, l_{ch}\sigma_c}$. Both $\Delta\alpha_c$ and $\bar{P}_f$ are defined by the intersection of these curves. In Fig. 12, the intersection points $(\alpha_0+\Delta\alpha_c, \frac{\bar{P}_f}{b\, l_{ch}\sigma_c})$ for each step of the CCFFM+LEBIM are depicted with different colours of filled circles. Note that if a crack grows up by a new segment $\Delta\alpha_c^i$ in an i-th step, the evaluation of the next crack growth starts at the crack length computed in the current i-th step $\alpha_0^i = \alpha_0^{i-1} + \Delta\alpha_c^i$, and so on.

As done in the previous section, the results have been compared with the solution in [33] (green line) in Figs. 12 and 13. Unlike the displacement control test, the failure of the interface using the coupled criterion is given by the intersection of the energy and the stress criteria curves in a finite segment of the interface. However, the solution in [33] is exactly the same as that by the original LEBIM with the critical energy defined in (7) and therefore the damage process is infinitesimal and is controlled only by the ERR.

It is also interesting to observe that considering Fig. 1, in the test under displacement control, the relative displacement at failure is δ_{max} for infinitesimal crack growth. However, under load control test, for a finite crack advance, the relative displacements at the failed zone along the interface (abruptly broken) are within an interval above δ_c. This observation shows that the crack growth by finite crack advances is also associated to a certain increase of the interface ductility (as described previously by other authors) when μ increases. Notice that relative displacements larger than δ_c are achieved at the crack tip before its damage. To illustrate this effect, the following maximum values of relative displacements at the crack tip before its damage are observed in the first finite crack advance: 1.65 δ_c for $\mu = 4$, 2.17 δ_c for $\mu = 8$ and 2.88 δ_c for $\mu = 16$.

Fig. 13 shows the variation of critical loads with respect to finite advances of the crack, each point is defined by $\Delta\alpha_c$ and $\frac{\bar{P}_f}{b\, l_{ch}\sigma_c}$ for each load step, until the end of the interface. Noteworthy, while in the DCB test under displacement control the crack propagation is stable, it is unstable under load control, as the failure load value decreases for subsequent crack advances, especially the failure load for the first crack advance is the highest failure load of all crack advances.

5.2. Solution obtained by the PMTE-SC

The procedure developed in this section is similar to that presented in Section 4.2. An important difference is that the potential energy variation of the system is $\Delta\Pi = \Delta U - \Delta W$, including the external-work term now. Therefore, the incremental energy balance for the DCB test under load control can be expressed as

$$\Delta U(\Delta a) - \Delta W(\Delta a) + \Delta R(\Delta a) \leq 0, \tag{67}$$

and $U(a) - W(a) + R(a)$ is minimized subjected to a stress condition.

5.2.1. Energy based formulation

In view of (49)-(50) and substituting the equations of the beam moment (18) and the stresses on the interface (17), the dimensionless elastic energy at AB zone can be written as

$$\hat{U}_{AB}(\alpha) = \frac{b\, l_{ch} 2k_n}{\bar{P}^2}\, U_{AB}(a) = \int_0^{\lambda-\alpha} \frac{1}{4}\left(\frac{\partial^2\hat{\sigma}(\xi,\alpha)}{\partial\xi^2}\right)^2 + (\hat{\sigma}(\xi,\alpha))^2\,\mathrm{d}\xi, \tag{68}$$

Where the first term of the integral is associated with the deformation of the two beams and the second term with the deformation of the interface. Recall that in the PMTE-SC approach, the energy expressions are presented for a specific configuration of the DCB which has a debonded zone α and a bonded zone $\lambda - \alpha$. To calculate the elastic energy of the BC zone, bending moment in BC zone is obtained by (52), giving

$$\hat{U}_{BC}(\alpha) = \frac{b\, l_{ch} 2k_n}{\bar{P}^2}\, U_{BC}(a) = \int_{\lambda-\alpha}^{\lambda} 4(\lambda-\xi)^2 \mathrm{d}\xi. \tag{69}$$

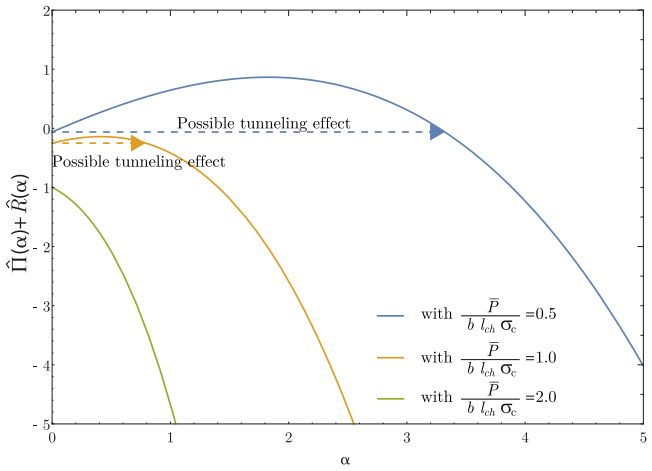

Fig. 14. Functions $\hat{\Pi}(\alpha)+\hat{R}(\alpha)$ for a specific dimensionless boundary condition in load $\frac{\bar{P}}{b\ l_{ch}\sigma_c}$, and $\mu = 8$.

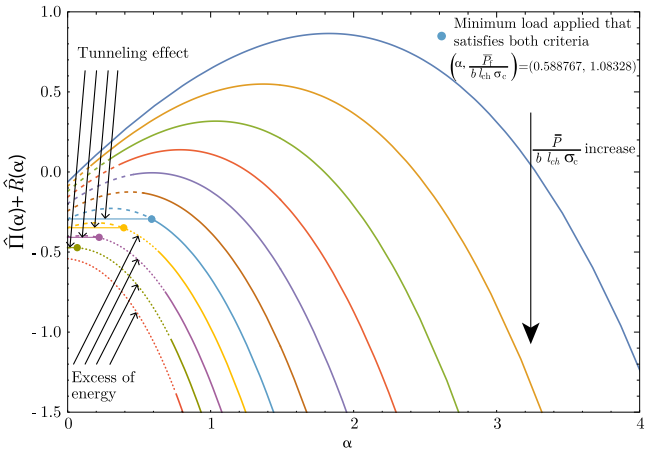

Fig. 15. Total energy function $\hat{\Pi}(\alpha) + \hat{R}(\alpha)$ for a specific dimensionless boundary condition in load $\frac{\bar{P}}{b\ l_{ch}\sigma_c}$. The dashed part of a curve represents the interface region of length α that fulfils the stress criterion.

The energy dissipated at this abrupt formation of a new crack and the total dissipated energy including the formation of the new crack on the interface are the same as under displacement control in (54).

To compute the external work $W(a)$ (the negative potential energy of the external loads) appearing in the definition of the potential energy $\Pi(a)$ and given by $W = 2\bar{P}u(\bar{P})$, the load applied at the end of the beams $\bar{P}$, and the displacement produced by these loads at the same point $u(\bar{P})$, are needed. To obtain this displacement, the procedure represented in Fig. 3 and explained in (30) is used, substituting adequately (17) in each definition of $w(x)$. Therefore $W(a)$ can be expressed as

$$W(a) = 2\bar{P}u(\bar{P}) = \frac{\bar{P}^2}{b\ l_{ch}2k_n}\left(2\hat{\sigma}(\lambda-\alpha,\alpha) + 2\alpha\frac{\partial\hat{\sigma}(\xi,\alpha)}{\partial\xi}\bigg|_{\lambda-\alpha} + \frac{8}{3}\alpha^3\right), \quad \text{with} \quad \hat{W}(\alpha) = \frac{b\ l_{ch}2k_n}{\bar{P}^2}W(a). \tag{70}$$

Note that $W(a) = 2U(a)$. This allows us to obtain a simpler expression of the total energy function to be minimized

$$\begin{aligned} U(a) - W(a) + R(a) &= \frac{\bar{P}^2}{b\ l_{ch}2k_n}\left(\hat{U}_{AB}(\alpha) + \hat{U}_{BC}(\alpha) - \hat{W}(\alpha)\right) + b\ l_{ch}G_{Ic}\alpha \\ &= b\ l_{ch}G_{Ic}\left(\frac{\bar{P}^2}{b^2\ l_{ch}^2\mu\ \sigma_c^2}\left(\hat{U}_{AB}(\alpha)\right.\right. \\ &\quad \left.\left.+\hat{U}_{BC}(\alpha) - \hat{W}(\alpha)\right) + \alpha\right) \\ &= b\ l_{ch}G_{Ic}\left(-\frac{\bar{P}^2}{2\ b^2\ l_{ch}^2\mu\ \sigma_c^2}\hat{W}(\alpha) + \alpha\right). \end{aligned} \tag{71}$$

The dimensionless form of this function writes as

$$-\hat{U}(\alpha) + \hat{R}(\alpha) = (-U(a) + R(a))\frac{1}{b\ l_{ch}G_{Ic}} = \left(-\frac{\bar{P}^2}{2\ b^2\ l_{ch}^2\mu\ \sigma_c^2}\hat{W}(\alpha) + \alpha\right). \tag{72}$$

The curves plotted in Fig. 14 are obtained by applying (72) using the parameters defined in Table 2 for different imposed loads at the ends of the beams and $\mu = 8$. This figure shows that the different curves provided by the energy balance are concave and $\hat{\Pi}(\alpha)+\hat{R}(\alpha) = -\hat{U}(\alpha) + \hat{R}(\alpha) \to -\infty$ for $\alpha \to \infty$. Thus, the global minimum of the total energy will coincide with its value for the largest possible value of α, i.e. $-\hat{U}(\lambda) + \hat{R}(\lambda)$, which corresponds to the total fracture of the specimen. However, the interface failure is only possible in zones where the stresses are high enough to satisfy the stress criterion. A consequence of the minimization of the total energy function, restricted only to the interface points subjected to sufficiently high stresses, is the prediction of crack onset as associated to a possible tunnelling through the total energy barrier for some load values, cf. [23]. See Fig. 14, where such situations are graphically illustrated by the curves for the lowest applied loads (represented by the blue and yellow lines). Such tunnelling effect is only allowed if all the interface points in the zone from $\alpha = 0$ to the intersection of the horizontal line with the curve of $-\hat{U}(\alpha) + \hat{R}(\alpha)$ verify the stress criterion. Note that, such tunnelling is possible because the energy condition $-\Delta U(a) + \Delta R(a) \leq 0$ is fulfilled. Nevertheless, in the case of the highest applied load (represented by the green line) the energy balance is fulfilled for any α, thus the size of the new crack segment would be given only by the stress criterion. In general, when the applied load increases, the zone needed to satisfy the stress criterion for tunnelling decreases, making easier the fracture onset.

5.2.2. Application of the PMTE-SC to a specific case and comparison between methods

To explain the PMTE-SC procedure for this DCB test, Fig. 15 shows the function $\hat{\Pi}(\alpha) + \hat{R}(\alpha) = -\hat{U}(\alpha) + \hat{R}(\alpha)$, for the geometrical and mechanical characteristics described in Table 2, $\mu = 8$ and $\alpha_0 = 0$. Similarly as in the DCB under displacement control, eleven different $\frac{\bar{P}}{b\ l_{ch}\sigma_c}$ values are used, ranging from 0.5 to 1.47, in intervals of 0.097. The ratio $\frac{\bar{P}}{b\ l_{ch}\sigma_c}$ represents the load imposed at the end of beams. For increasing values of $\frac{\bar{P}}{b\ l_{ch}\sigma_c}$, the initial values of the total energy, for $\alpha = 0$, and also its maxima decrease. The zone of possible interface fracture is given by undamaged interface points satisfying the stress criterion (65). Thus, tunnelling the total energy barrier is only possible for a given α verifying $\hat{\Pi}(\alpha)+\hat{R}(\alpha) = \hat{\Pi}(0)+\hat{R}(0)$ if all interface points ξ, $\lambda - \alpha \leq \xi \leq \lambda$, fulfil the stress criterion.

The interface zones that satisfies (65) are represented in Fig. 15 by dashed lines. As expected, for increasing $\frac{\bar{P}}{b\ l_{ch}\sigma_c}$ the zone that fulfils the stress criterion also increases, from the first curve, where no point verifies the stress criterion, to the last curve, which has the largest zone where fracture is possible. Although this zone increases with the applied load, it can be seen that in the first six curves the interface fracture cannot occur according to the PMTE-SC, since $\Delta\hat{\Pi}(\alpha)+\Delta\hat{R}(\alpha) > 0$ for the largest value of α fulfilling the stress criterion. However, the load associated to the seventh curve (light blue) allows a crack onset by tunnelling through the total energy barrier because $\Delta\Pi(\Delta a_c)+\Delta R(\Delta a_c) = 0$. It should be stressed that this configuration represents the minimum load applied that satisfies both stress and energy criteria. In the next

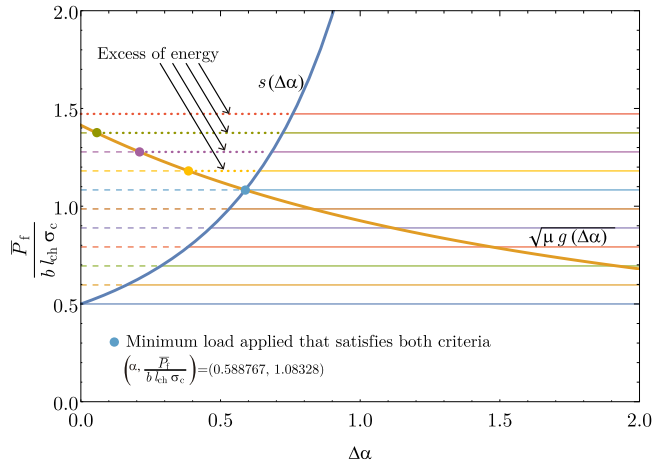

Fig. 16. Comparison of the Δa_c value predicted using PMTE-SC and the stress and energy criteria curves methodology. Horizontal lines represent the applied dimensionless loads $\frac{\bar{P}}{b\, l_{ch}\sigma_c}$ included in Fig. 15 to make easy connections between these figures.

three curves, the applied loads allow the damage due to tunnelling through the total energy barrier and subsequent unstable crack growth due to an excess of energy, because $\Delta\Pi(\Delta a_c) + \Delta R(\Delta a_c) < 0$. In the last curve, for the largest load considered, only unstable crack growth is predicted, this observation can be explained by the fact that, for a linear elastic interface, a nonzero ERR, $G > 0$, is obtained even in configurations with no pre-crack, i.e. $\alpha_0 = 0$.

For a better understanding of the results obtained by the PMTE-SC included in Fig. 15, a comparison with the CCFFM+LEBIM using the stress and energy criteria curves methodology developed in Section 5.1 is carried out. Fig. 16 plots the curves $s(\Delta\alpha)$ and $\sqrt{\mu\ g(\Delta\alpha)}$ for $\mu = 8$, as in Section 5.1. Eleven horizontal lines have been added which coincide with the $\frac{\bar{P}}{b\, l_{ch}\sigma_c}$ values and colours used in Fig. 15. The intersection of these horizontal lines with the curve $s(\Delta\alpha)$ is indicated by the change from dashed to continuous lines. These dashed lines define, for each $\frac{\bar{P}}{b\, l_{ch}\sigma_c}$ value, the length of the region $\Delta\alpha$ that satisfies the stress criterion. The lengths of the regions subjected to sufficiently high stresses coincide perfectly with the end of the dashed lines in Fig. 15. It is interesting to note, that from the seventh horizontal line (light blue) the next horizontal lines also intercept the energy criterion curve at values higher than the stress criterion. This light blue point defines the minimum load that satisfies both criteria. Noteworthy, all higher loads produce an excess of energy which leads to unstable crack growth at the interface and it is represented by the dotted lines within the dashed lines.

6. Conclusions

In the present study an insight into the coupled criterion of Finite Fracture Mechanics (CCFFM) is presented by analysing two alternative approaches: (a) the traditional method based on intersection of stress and energy criteria curves and (b) the novel Principle of Minimum Total Energy subjected to a Stress Condition (PMTE-SC) introduced in [23]. Recall that CCFFM assumes the possibility of a damage mechanism leading to the onset of a new finite segment of crack. Therefore, it releases Griffith's hypothesis assuming that crack growth is infinitesimal.

These two approaches to CCFFM are applied to the well-known DCB test for isotropic materials with a thin adhesive layer, as reference problem. The present analysis includes a discussion of the effect of displacement or load control on crack growth. Analytical solutions based on Euler–Bernoulli's beams bonded by a spring interface are used for both configurations. A deep study of the energies behaviour in the DCB test under displacement and load control is presented. As expected, stable and unstable crack growth, respectively, is predicted for displacement and load control. Specifically, for the test under displacement control an infinitesimal crack growth on the interface is predicted, reverting the CCFFM predictions to those based on Griffith's hypothesis. In the test under load control, failure occurs in the whole interface when the critical load is reached.

In all studied cases, both CCFFM methodologies provide identical analytical predictions for fracture, showing that the PMTE-SC is equivalent to the classical formulation of the CCFFM. Moreover, the analysis for DCB under load control by PMTE-SC indicates that typical CCFFM predictions of finite crack onset are in fact associated to a tunnelling effect of the total energy barrier, as suggested in [23]. Actually the main objective of the presented study is to analyse this new methodology for the prediction of damage onset and propagation. The present results open up new possibilities for PMTE-SC, as this approach could be more versatile when implemented in FEM codes by an incremental load stepping scheme, and it could be applied to more complex configurations including multiple cracks initiating and propagating under mixed mode. Noteworthy, that in fracture mixed mode, G_c does not remain constant and may change depending on the crack advance.

CRediT authorship contribution statement

M. Muñoz-Reja: Data curation, Formal analysis, Funding acquisition, Investigation, Methodology, Software, Validation, Writing – original draft, Writing – review & editing. **V. Mantič:** Conceptualization, Formal analysis, Funding acquisition, Investigation, Methodology, Resources, Supervision, Validation, Writing – original draft, Writing – review & editing. **L. Távara:** Formal analysis, Funding acquisition, Investigation, Resources, Supervision, Validation, Writing – original draft, Writing – review & editing.

Declaration of competing interest

The authors declare that they have no known competing financial interests or personal relationships that could have appeared to influence the work reported in this paper.

Acknowledgements

The authors would like to express their gratitude to Dr. Christos Panagiotopoulos (Hellenic Mediterranean University, Greece) for stimulating this research and productive discussions. The present work was supported by Spanish Ministry of Science, Innovation and Universities and European Regional Development Fund (Project PGC2018-099197-B-I00), Consejería de Economía *y* Conocimiento de la Junta de Andalucía, Spain (Project P18-FR-1928 and Contract US-1266016-Programa Operativo FEDER Andalucía 2014–2020), Junta de Andalucía, Spain and European Social Fund (Acciones de transferencia del conocimiento AT17-5908-USE).

References

[1] Z. Hashin, Finite thermoelastic fracture criterion with application to laminate cracking analysis, J. Mech. Phys. Solids 44 (7) (1996) 1129–1145.
[2] D. Leguillon, Strength or toughness? A criterion for crack onset at a notch, Eur. J. Mech. A Solids 21 (2002) 61–72.
[3] D. Taylor, P. Cornetti, N. Pugno, The fracture mechanics of finite crack extension, Eng. Fract. Mech. 72 (2005) 1021–1038.
[4] P. Cornetti, N. Pugno, A. Carpinteri, D. Taylor, Finite fracture mechanics: a coupled stress and energy failure criterion, Eng. Fract. Mech. 73 (2006) 2021–2033.
[5] P.P. Camanho, C.G. Davila, M.F. de Moura, A finite fracture mechanics model for the prediction of the open-hole strength of composite laminates, Compos. A 43 (8) (2012) 1219–1225.

[6] A. Sapora, P. Cornetti, A. Carpinteri, D. Firrao, An improved finite fracture mechanics approach to blunt V-notch brittle fracture mechanics: Experimental verification on ceramic, metallic, and plastic materials, Theor. Appl. Fract. Mech. 78 (2015) 20–24.
[7] I.G. García, V. Mantič, A. Blázquez, The effect of residual thermal stresses on transverse cracking in cross-ply laminates: an application of the coupled criterion of the finite fracture mechanics, Int. J. Fract. 211 (2018) 61–74.
[8] P. Rosendahl, Y. Staudt, A. Schneider, J. Schneider, W. Becker, Nonlinear elastic finite fracture mechanics: Modeling mixed-mode crack nucleation in structural glazing silicone sealants, Mater. Des. 182 (2019) 108057.
[9] A. Doitrand, A. Sapora, Nonlinear implementation of finite fracture mechanics: A case study on notched Brazilian disk samples, Int. J. Non-Linear Mech. 119 (2020) 103245.
[10] A. Doitrand, P. Cornetti, A. Sapora, R. Estevez, Experimental and theoretical characterization of mixed mode brittle failure from square holes, Int. J. Fract. 228 (2021) 33–43.
[11] L. Prandtl, A thought model for the fracture of brittle solids, Z. Phys. Angew. Math. Mech. 13 (2) (1933) 129–133.
[12] V. Entov, R. Salganik, On the Prandtl brittle fracture model, Mech. Solids 3 (1968) 79–89, (translated from Russian).
[13] S. Lenci, Analysis of a crack at a weak interface, Int. J. Fract. 108 (2001) 275–290.
[14] A. Carpinteri, P. Cornetti, N. Pugno, Edge debonding in FRP strengthened beams: Stress versus energy failure criteria., Eng. Struct. 31 (2009) 2436–2447.
[15] L. Távara, V. Mantič, E. Graciani, J. Cañas, F. París, Analysis of a crack in a thin adhesive layer between orthotropic materials. An application to composite interlaminar fracture toughness test, CMES-Comput. Model. Eng. Sci. 58 (3) (2010) 247–270.
[16] L. Távara, V. Mantič, E. Graciani, F. París, BEM analysis of crack onset and propagation along fiber-matrix interface under transverse tension using a linear elastic-brittle interface model, Eng. Anal. Bound. Elem. 35 (2011) 207–222.
[17] V. Mantič, L. Távara, A. Blázquez, E. Graciani, F. París, A linear elastic - brittle interface model: Application for the onset and propagation of a fibre-matrix interface crack under biaxial transverse loads, Int. J. Fract. 195 (2015) 15–38.
[18] P. Cornetti, V. Mantič, A. Carpinteri, Finite fracture mechanics at elastic interfaces, Int. J. Solids Struct. 49 (2012) 1022–1032.
[19] M. Muñoz Reja, L. Távara, V. Mantič, P. Cornetti, Crack onset and propagation at fibre-matrix elastic interfaces under biaxial loading using finite fracture mechanics, Compos. A 82 (2016) 267–278.
[20] M. Muñoz Reja, L. Távara, V. Mantič, Convergence of the BEM solution applied to the CCFFM for LEBIM, Key Eng. Mater. 774 (2018) 355–360.
[21] M. Muñoz Reja, P. Cornetti, L. Távara, V. Mantič, Interface crack model using finite fracture mechanics applied to the double pull-push shear test, Int. J. Solids Struct. 188–189 (2020) 56–73.
[22] M. Muñoz Reja, L. Távara, V. Mantič, P. Cornetti, A numerical implementation of the coupled criterion of finite fracture mechanics for elastic interfaces, Theor. Appl. Fract. Mech. 108 (2020).
[23] V. Mantič, Prediction of initiation and growth of cracks in composites. Coupled stress and energy criterion of the finite fracture mechanics (Keynote lecture), in: Proceedings of the 16th European Conference on Composite Materials (ECCM16), F. París (Ed.), 2014, http://www.escm.eu.org/eccm16/assets/1252.pdf.
[24] R. Dimitri, P. Cornetti, V. Mantič, M. Trullo, L.D. Lorenzis, Mode-I debonding of a double cantilever beam: A comparison between cohesive crack modeling and finite fracture mechanics, Int. J. Solids Struct. 124 (2017) 57–72.
[25] P.L. Rosendahl, P. Weißgraeber, Modeling snow slab avalanches caused by weak layer failure – Part I: Slabs on compliant and collapsible weak layers, Cryosphere Discuss. (2019) 1–28.
[26] V. Mantič, Interface crack onset at a circular cylindrical inclusion under a remote transverse tension. Application of a coupled stress and energy criterion, Int. J. Solids Struct. 46 (2009) 1287–1304.
[27] I.G. García, M. Paggi, V. Mantič, Fiber-size effects on the onset of fiber-matrix debonding under transverse tension: A comparison between cohesive zone and finite fracture mechanics models, Eng. Fract. Mech. 115 (2014) 96–110.
[28] A.C. Garg, Delamination - A damage mode in composite structures, Eng. Fract. Mech. 29 (1988) 557–584.
[29] T. Tay, Characterization and analysis of delamination fracture in composites: An overview of developments from 1990 to 2001, Appl. Mech. Rev. 56 (2003) 1–31.
[30] O. Volkersen, Die Nietkraftverteilung in Zugbeanspruchten Nietverbindungen mit Konstanten Laschen-querschnitten, Luftfahrtforschung 15 (1938) 4–47.
[31] M. Goland, E. Reissner, The stresses in cemented joints, J. Appl. Mech. 11 (1944) A17–A27.
[32] M.F. Kanninen, An augmented double cantilever beam model for studying crack propagation and arrest, Int. J. Fract. 9 (1973) 83–92.
[33] L. Škec, G. Alfano, G. Jelenić, Complete analytical solutions for double cantilever beam specimens with bi-linear quasi-brittle and brittle interfaces, Int. J. Fract. 215 (2019) 1–37.
[34] S. Wolfram, The Mathematica Book, Wolfram Media, 2003.